Journal of Power Sources 280 (2015) 182–189

Contents lists available at ScienceDirect

Journal of Power Sources

journal homepage: www.elsevier.com/locate/jpowsour

Failure mechanism for flexible dye-sensitized solar cells under repeated outward bending: Cracking and spalling off of nano-porous titanium dioxide film

Xue-Long He [a], Guan-Jun Yang [b, *], Chang-Jiu Li [b, *], Mei Liu [b], Sheng-Qiang Fan [c]

[a] Jiangxi Province Key Laboratory of Precision Drive and Control, Nanchang 330099, PR China
[b] State Key Laboratory for Mechanical Behavior of Materials, School of Materials Science and Engineering, Xi'an Jiaotong University, Xi'an, Shaanxi 710049, PR China
[c] School of Chemistry & Molecular Biosciences, The University of Queensland, QLD 4072, Australia

HIGHLIGHTS

- Performance of solar cell under multiple outward bending was systematically studied.
- Cracking and spalling off of TiO_2 film are responsible for failure of solar cell.
- A failure model for flexible DSCs under repeated outward bending was proposed.

GRAPHICAL ABSTRACT

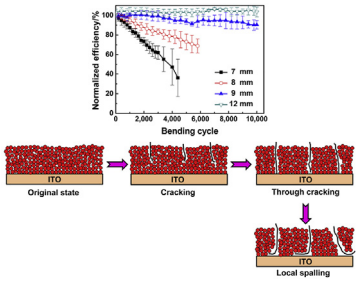

ARTICLE INFO

Article history:
Received 21 October 2014
Received in revised form
15 December 2014
Accepted 14 January 2015
Available online 14 January 2015

Keywords:
Dye-sensitized solar cells
Failure mechanism
Electrochemical impedance spectroscopy
Outward bending

ABSTRACT

Flexibility, as well as efficiency, of flexible dye-sensitized solar cells (DSCs) is of significant importance to their applications. In this study, quantitative bending test, carried out with a lab-developed solar cell bending tester, is used to simulate the flexible service condition. The photovoltaic performance, morphology of the photoanode and electrochemical property evolution during bending service are examined to aim at understanding the bending failure mechanism for the flexible DSCs under repeated outward bending (the TiO_2 film in the photoanode is in tension). Results show that when the bending radius is 12 mm, the efficiency of the plastic DSCs keeps unchanged with increasing the bending cycle. When the bending radius is smaller than 12 mm, the efficiency of the flexible DSCs decreases with increasing the bending cycle. The electrochemical impedance spectroscopy results show that the increase of the electron transport resistance (R_t) in TiO_2 network is responsible for the degradation of efficiency. Furthermore, the photoanodes after repeated bending is cracking and spalling off from the ITO surface. Finally, a failure model for the flexible DSCs under repeated outward bending is proposed.

1. Introduction

Recently, there is an increasing interest in replacing the rigid glass-based dye-sensitized solar cells (DSCs) by plastic substrates due to light-weight, flexibility of shape, suitability for low cost roll-to-roll production [1,2]. However, owing to the low heat-resistance

* Corresponding authors.
E-mail addresses: ygj@mail.xjtu.edu.cn (G.-J. Yang), licj@mail.xjtu.edu.cn (C.-J. Li).

http://dx.doi.org/10.1016/j.jpowsour.2015.01.088
0378-7753/

temperature (150 °C) of the plastic substrates, the high-temperature annealing methods used on conventional glass-based DSCs are not applicable. The TiO_2 film prepared by low-temperature methods showed poor particle–particle connection. Therefore, low efficiency and low bending performance were two basic problems which restricted the industrial applications of the flexible DSCs [3,4].

Over the last few years, in order to improve the particle–particle connection of the TiO_2 films on plastic substrates, a couple of low-temperature methods have been developed, including mechanical compression [5,6], microwave irradiation [7], hydrothermal crystallization [8], chemical sintering [9,10], electron-beam annealing [11], electrophoretic deposition [12] and room temperature cold spraying [13,14]. Up to now, the highest efficiency of the assembled flexible DSCs has been up to 8.1%, which is nearly 80% of the conventional glass-based DSCs [15].

However, the flexibility, one of the most important parameters of the flexible DSCs, is rarely reported to our knowledge. Jiang et al. [16] used ZnO nanowire to replace ZnO nanoparticle as the photoanode for flexible DSCs. The nanowire-based photoanode endured bending 2000 cycles with a bending radius of 2 mm, the assembled flexible DSC showed nearly unchanged efficiency. Meanwhile, the nanoparticle-based photoanode endured bending 5 cycles, the efficiency of the assembled flexible DSC decreased by 75%. Li et al. [17] also improved the flexibility by blending elastic polymer PMMA with TiO_2 nanoparticles, though the efficiency was decreased by the introduction of polymer in TiO_2 film.

For most of the studies until now, the bending performance was obtained by bending the photoanodes firstly and then measuring the performance of the assembled flexible DSCs. It should be noted that, bending photoanode is totally different from bending solar cell. After bending the photoanode, the subsequently dye absorption and assembly of solar cell may bring unpredictable effects to the performance of the flexible DSCs. Therefore, bending solar cell becomes imperative.

In this study, the TiO_2 nanocrystalline layer was prepared by room temperature cold spray method (RTCS, also called vacuum cold spray method). The bending service behavior of the flexible DSCs under repeated outward bending was examined to aim at understanding the multiple bending failure mechanism for the flexible DSCs.

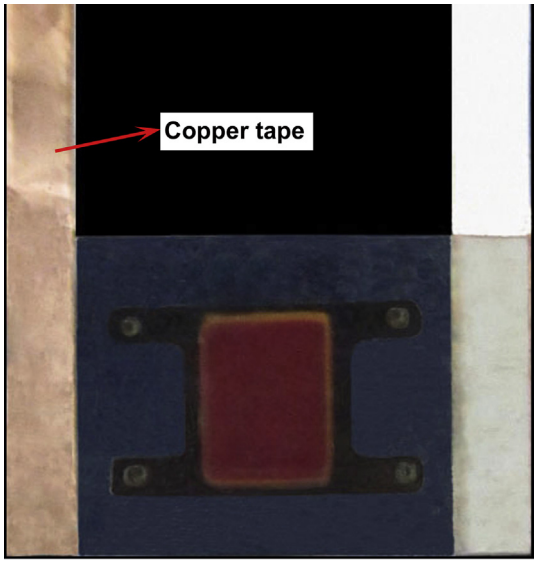

Fig. 1. The photograph of the flexible DSC.

2. Experimental

2.1. Preparation of flexible DSCs

The TiO_2 film was prepared by a home-developed room temperature cold spray system [18] using a commercial TiO_2 powder (P25, Degussa, 70% anatase and 30% rutile) with a thickness of 10 μm on ITO-PEN plastic substrate (PECF-IP, 15 Ω sq^{-1}, Peccell). The electrode was heated at 135 °C for 15 min. After cooled to 80 °C, the electrode was immersed in an absolute ethanol solution containing 0.3 mM N719 dye (Solaronix) for 24 h, then rinsed with absolute ethanol and dried with nitrogen gas. The photoanode was then used to assemble the solar cell with a plastic-based Pt counter electrode (CE) using a 60 μm thick Surlyn film (1702, DuPont) spacer. Current collector contacts made of copper tape were placed on both sides of the cell. The electrolyte solution was introduced into the cell through four holes pre-drilled on the back of the CE, and then the holes were sealed up using an UV resin (ThreeBond). The electrolyte solution was composed of 0.6 M DMPII (Institute of Plasma Physics), 0.05 M I_2 (Aldrich), 0.1 M LiI (Aldrich), and 0.5 M 4-*tert*-butylpyridine (Acros) in dehydrated acetonitrile (Aldrich). Fig. 1 shows the photograph of the flexible DSC.

2.2. Characterization of photovoltaic performance and electrochemical properties of flexible DSCs

The bending test was carried out by a home-developed flexible solar cell bending tester, by which the bending condition, including bending mode, bending radius and bending cycle, were accurately and automatically controlled [19,20]. Fig. 2 shows the photograph of the bending tester used to bend the solar cell. Fig. 3 shows a bending cycle of the flexible DSC under outward bending mode. The TiO_2 photoanode is in tension while under outward bending state, which will be discussed in the following section.

The photovoltaic performance of flexible DSCs was measured using a solar simulator (100 mW cm^{-2}, Oriel 94023A, Newport) equipped with a Keithley 2400 digital source meter. The area of the photoanode was controlled to be 0.48 cm^2. The electrochemical properties of the flexible DSCs were investigated by electrochemical impedance spectroscopy (EIS). The EIS spectra were measured in the dark at −0.7 V bias potential using a CHI606 electrochemical workstation (Shanghai Chenhua Instrument, China). The spectra were scanned in a frequency ranging from 10^{-1}–10^5 Hz with an ac amplitude of 10 mV. The obtained impedance spectra were fitted with the Z-view software in terms of appropriate equivalent circuit model [21,22].

2.3. Characterization of the TiO_2 film structure

In order to examine the structure evolution of the photoanode under repeated outward bending, the photoanodes were detached from the tested DSCs, rinsed with acetonitrile and ethanol sequentially to remove the electrolyte, and then observed by a field emission scanning electron microscope (FESEM, QUANTA 600F). Besides, there might be through cracks along in-plane direction in the photoanode, which are difficult to be observed by the optical microscope. Therefore, high resolution transmission electron microscope (HRTEM, JEM-2100 F) was used to observe the state of through cracks, which actually acted as a high resolution optical microscope. Fig. 4 shows the preparation process of the specimen for HRTEM observation. The TiO_2 film was immersed in a 0.1 M HCl solution for 24 h to etch the ITO film from the photoanode. The TiO_2 film was rinsed with ethanol and then heated at 100 °C for 10 min. Finally, the TiO_2 film with suitable size was fixed by two copper gauzes, and then observed by the HRTEM.

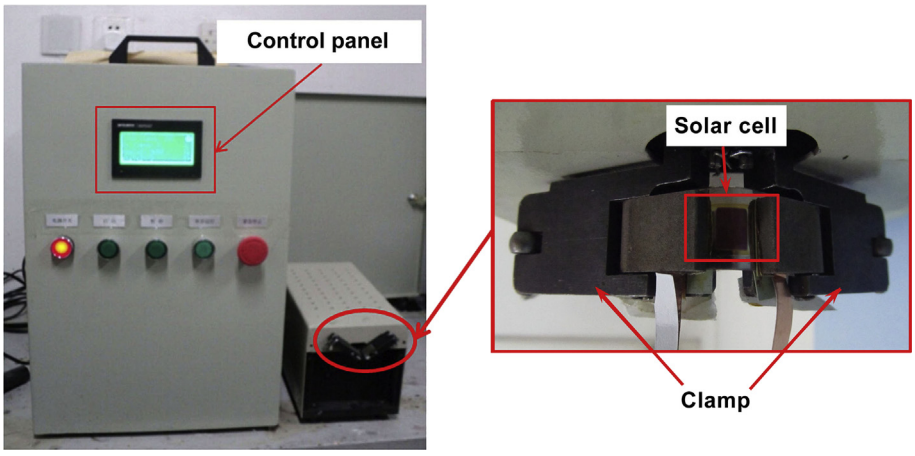

Fig. 2. The bending tester used to bend the flexible DSC.

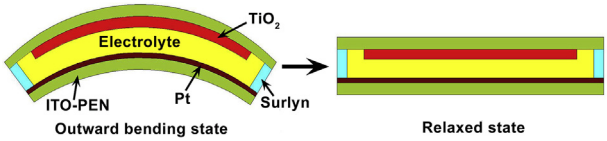

Fig. 3. A bending cycle of the flexible DSC under outward bending mode.

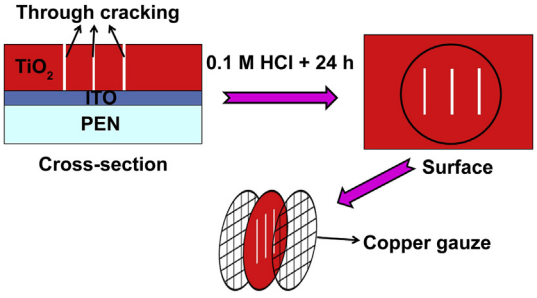

Fig. 4. Schematic for the preparation process of the specimen for HRTEM observation.

3. Results and discussion

3.1. Analysis of the position of the neutral layer in flexible DSC

To determine the position of the neutral layer of the flexible DSC, the thickness and the elastic modulus (E) of the constituents in the flexible DSC should be given. In this study, the elastic modulus of the constituents was calculated from the results of tiny force tensile test (MTS Tytron250).

Fig. 5 shows the stress–strain curve and fitting results of the PEN film. By fitting the linear portion of the stress–strain curve, the elastic modulus of the PEN film is calculated as 5.4 ± 0.2 GPa, which is comparable to the data (4–5 GPa) in literature [23].

Compared to the thickness of the PEN film (200 μm), the thickness of the deposited ITO film (0.3 μm) and TiO_2 film (10 μm) is relatively small. It is difficult to obtain the stress–strain curve of the ITO and TiO_2 film by tiny force tensile test directly. Therefore, in this study, a strength separation method based on the Hooke's law is used. In the elastic deform portion of the ITO-PEN film, the force on the ITO film can be calculated by $F_{ITO}=F_{ITO\text{-}PEN} - F_{PEN}$. Therefore, after calculating, the stress–strain curve of ITO film can be obtained, as shown in Fig. 6(a). By fitting the linear portion in the

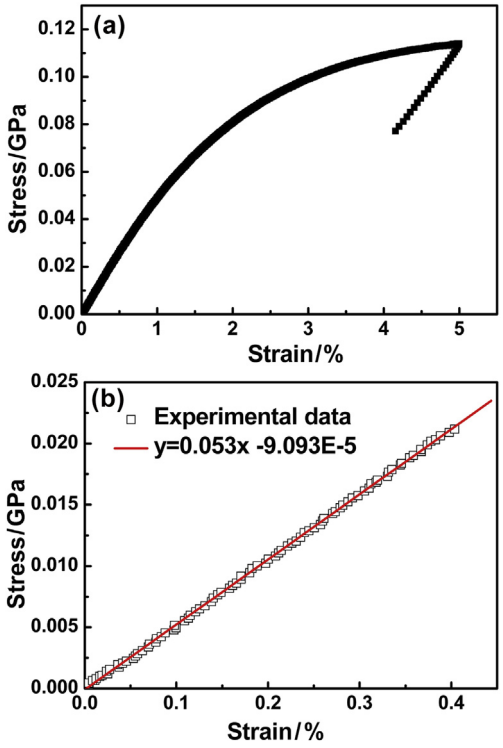

Fig. 5. Stress-strain curve (a) and fitting results (b) of the PEN film.

curve (Fig. 6(b)), the elastic modulus of the ITO film is calculated as 185 ± 5 GPa.

By using the same way, the elastic modulus of the TiO_2 film can be obtained. Fig. 7 shows the elastic modulus of the TiO_2 film with different thicknesses. From Fig. 7, it is found that the elastic modulus is independent on the thickness of TiO_2 film, thereby the elastic modulus of the TiO_2 film in this study is the average value 9 ± 3 GPa. However, Diebold [24] shows the elastic modulus of the TiO_2 bulk is 244–289 GPa. This result shows that the high porosity (ca. 50%) in the nano-porous TiO_2 film notably decreases the deformation resistance.

The thickness of the different layers in photoanode is quite different, i.e. 200 μm PEN film, 0.3 μm ITO film, 10 μm TiO_2 film, and 0.1 μm Pt film. Considering the size of the photoanode (6 mm × 8 mm) is nearly 20 times of the cell thickness (446.7 μm),

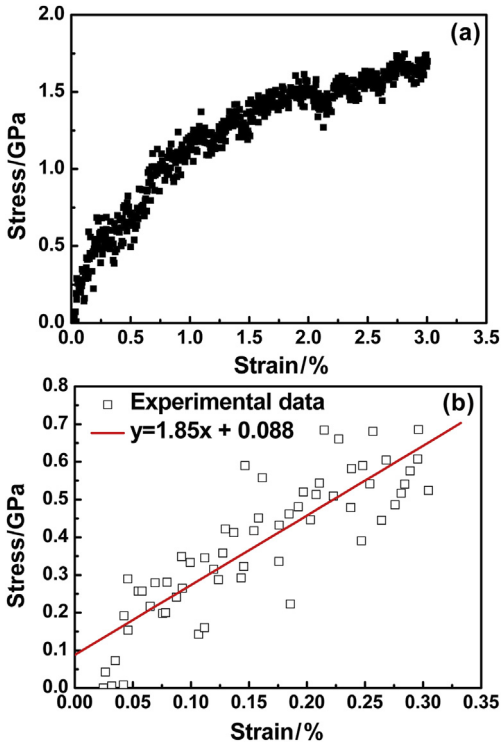

Fig. 6. Stress-strain curve (a) and fitting results (b) of the ITO film.

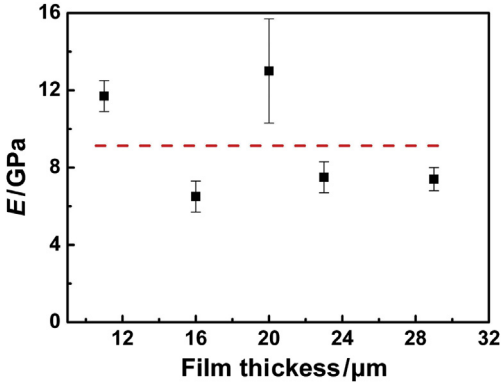

Fig. 7. Influence of film thickness on the elastic modulus of the TiO_2 film.

the solar cell system can be appropriately simplified to an infinite large plate. The liquid electrolyte in the solar cell can be regarded as incompressible liquid phase. Fig. 8 shows the coordinate system of the flexible DSC. The origin of z axis in the coordinate is defined as the ITO/TiO_2 interface. The position of the neutral layer can be calculated by the following formula:

$$Z_0 = \frac{\int_{Z_1}^{Z_2} zE(z)dz}{\int_{Z_1}^{Z_2} E(z)dz} \quad (1)$$

where Z_0 is the position of the neutral layer in Z coordinate. After calculation, Z_0 is 22.53 μm, that is, the distance between the neutral layer and the ITO/TiO_2 interface is 22.53 μm.

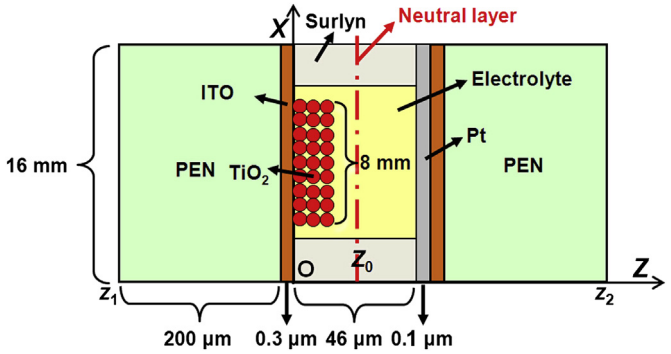

Fig. 8. The coordinate system of the flexible DSC.

3.2. Stress analysis of the TiO_2 film in the flexible DSC

After determining the position of the neutral layer in the flexible DSC, the strain of the TiO_2 film in flexible DSC can be calculated by the following formula:

$$\varepsilon = \frac{Z_0 - z}{R} \quad (2)$$

where ε is the strain, z is the position of the TiO_2 film, R is the bending radius.

For the whole TiO_2 film with a thickness of 10 μm, it is obvious that different detailed parts of the film present different distance from the neutral layer and thereby different strain and stress. Fig. 9 shows the influence of bending radius on the strain and stress of the TiO_2 film. Herein three typical parts are listed, i.e. top part (TiO_2 film surface), middle part and bottom part (ITO/TiO_2 interface) in Fig. 9. It can be found that the strain and stress in top part is minimum and those in bottom part is maximum. The strain and

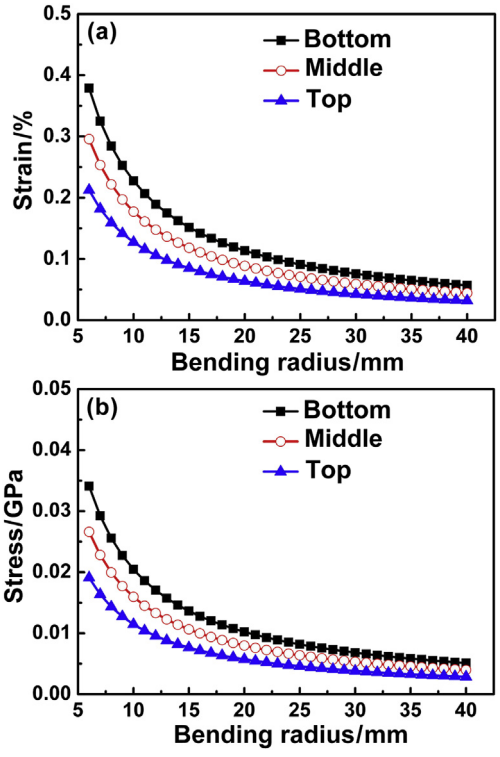

Fig. 9. Influence of bending radius on the strain (a) and stress (b) of the TiO_2 film.

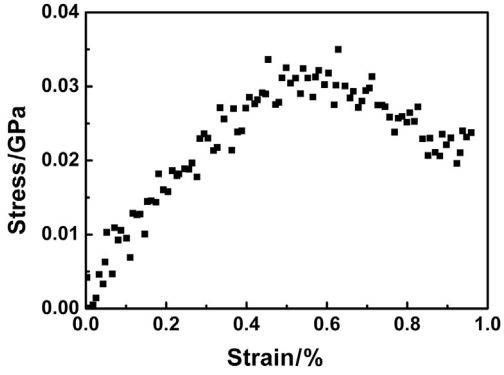

Fig. 10. Stress-strain curve of the TiO_2 film.

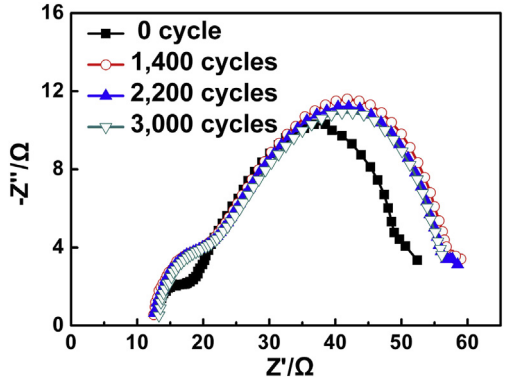

Fig. 12. Typical Nyquist plots of the flexible DSCs after different bending cycles (R = 7 mm).

stress of the TiO_2 film increases with decreasing the bending radius. The maximum strain of the top part of the TiO_2 film is 0.37%. The strain and stress in the middle part of the film can be an average of the whole thickness of the TiO_2 film. Fig. 10 shows stress–strain curve of the TiO_2 film obtained by the tiny force tensile test. From Fig. 10, the TiO_2 film is in elastic deformation stage when the strain of TiO_2 film is less than 0.5%, which is much larger than the maximum strain of 0.37% in the TiO_2 film even if the solar cell is subjected to the bending test at a bending radius of 6 mm in this study. This result shows that the TiO_2 film will not crack under single bending, which is in accord with the results in our previous study [19]. However, under the repeated bending condition, whether the TiO_2 film will crack or even spall off should be carefully examined, since the mechanical behavior of materials under single loading and repeated loading is different.

3.3. Bending service behavior of flexible DSCs under repeated outward bending

Before the bending test, the photovoltaic parameters of the assembled flexible DSCs were measured. The short-circuit current density (J_{SC}) is 8 mA cm^{-2}, the open-circuit photovoltage (V_{OC}) is 0.70 V, the fill factor (FF) is 0.68, and the energy conversion efficiency is 3.8%.

It should be noted that, there are four factors which may affect the performance of the flexible DSC during bending test, namely, the electrical property degradation of the ITO-PEN film, the electrocatalytic property degradation of the Pt CE, the leak of electrolyte and the failure of TiO_2 film. During the bending test, the leak of electrolyte is found, which is just technique problem and beyond the scope of this study. It's should be note that, in order to eliminate the influence of electrolyte leakage on the photovoltaic performance of the DSCs, once the electrolyte leakage appeared during the bending test, the experiment data of this particular solar cell was not used in this study. For the Pt CE, our recently results show that the electrocatalytic property of the Pt CE does not decrease after repeated bending. Therefore, the ITO-PEN film and the TiO_2 film can be responsible for the performance degradation of flexible DSC.

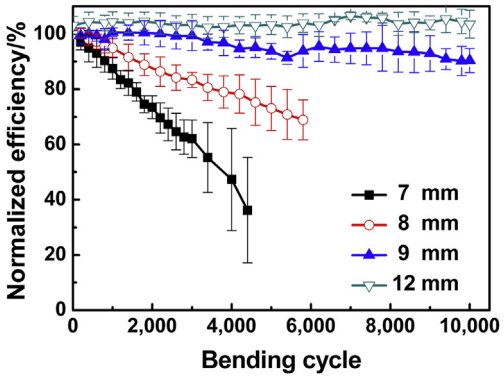

Fig. 11. Influence of bending radius and bending cycle on the normalized efficiency of flexible DSCs.

Fig. 11 shows the influence of bending radius and bending cycle on the normalized efficiency of the flexible DSCs. When the bending radius is 12 mm, the normalized efficiency (compared to the efficiency of the original flexible DSC) of the flexible DSCs keeps unchanged with increasing the bending cycle. When the bending radius is smaller than 12 mm, the normalized efficiency decreases with increasing the bending cycle. The smaller the bending radius, the lower the efficiency of the flexible DSCs after the same bending cycle.

In order to investigate the reason for the degradation of the solar cell, the electrochemical properties of the solar cell were investigated by EIS. The flexible DSC with a bending radius of 7 mm was chose as an example. Fig. 12 shows the typical Nyquist plots of the flexible DSCs after different bending cycles. As shown in Fig. 12, two arcs can be assigned to the transport process of the electrons at the interface of Pt/electrolyte and TiO_2/electrolyte, respectively, from left to right. By fitting the EIS data using a Z-view software with a generalized equivalent circuit model [21,22], the electrochemical properties can obtained as listed in Table 1. From Table 1, the series resistance (R_s), which is the sum of two conductive substrates and the resistance of external circuits, nearly the same with increasing the bending cycle. This means the ITO-PEN film is not responsible for the performance degradation of the flexible DSCs. Therefore, the TiO_2 film is responsible for the performance degradation of flexible DSCs. The charge transfer resistance (R_{ct}), which relates to the electron recombination at the TiO_2/electrolyte interface, also keeps unchanged with increasing the bending cycle. However, the electron transport resistance (R_t) in the TiO_2 film increases with

Table 1
Electrochemical property of the flexible DSCs after different bending cycles (R = 7 mm).

Bending cycle	R_s (Ω)	R_{ct} (Ω)	R_t (Ω)
0 cycle	11.5	34.4	14.8
1400 cycles	10.8	35.9	28.4
2200 cycles	11.0	34.5	28.1
3000 cycles	11.8	33.1	31.2

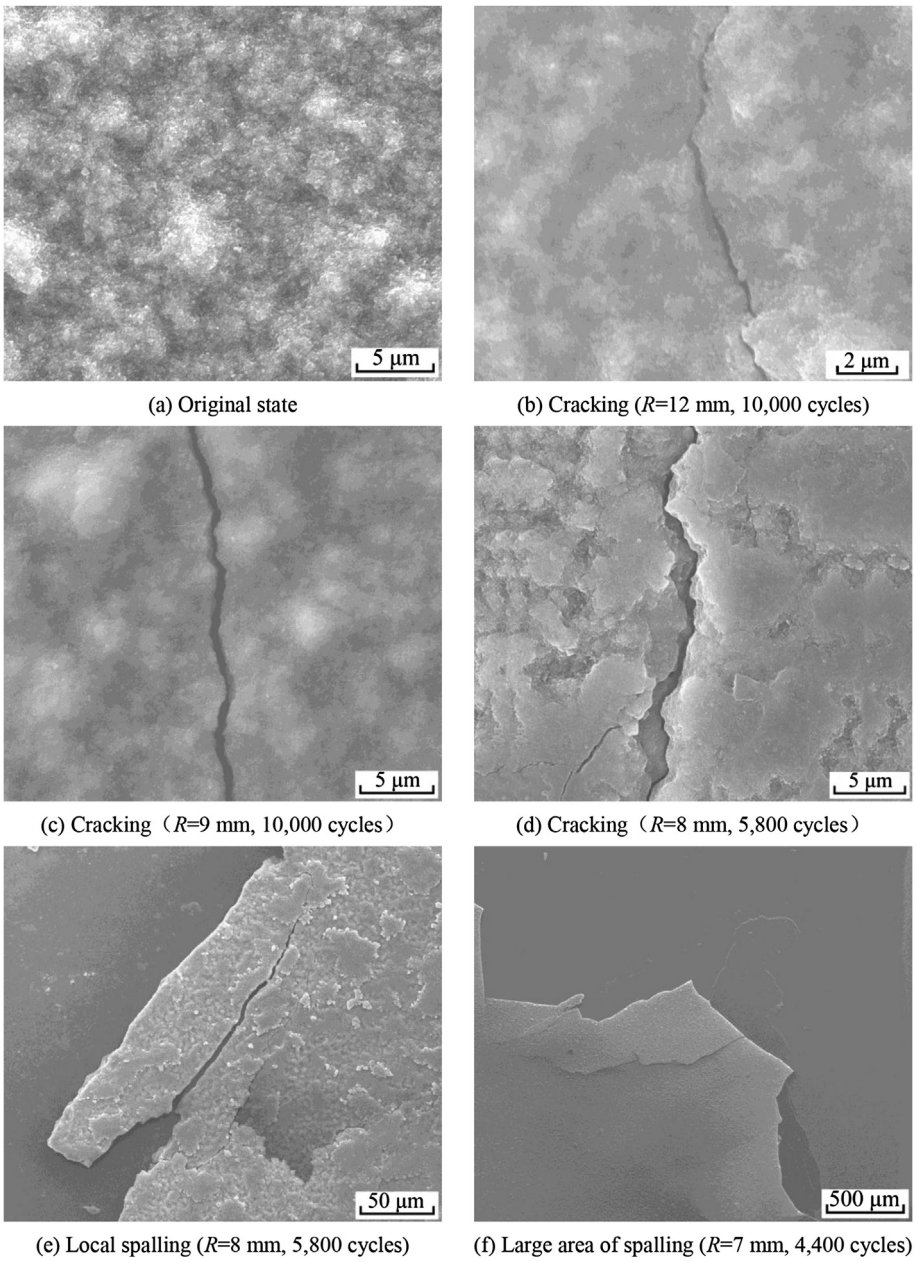

Fig. 13. Surface morphologies of the photoanodes in flexible DSCs after different bending conditions.

increasing the bending cycle. After 3000 cycles outward bending, the R_t value is more than two times of the R_t value of the original solar cell. Therefore, from the perspective of electrochemistry, the increase of R_t is responsible for the degradation of flexible DSC after repeated outward bending. Since the R_t relates to the particle–particle connection in the TiO_2 film, it is confirmed that the connection between the particle and particle in TiO_2 film is damaged after repeated outward bending, resulting in the decrease of electron collection efficiency and thereby the decrease of energy conversion efficiency of the flexible DSCs.

Besides, in order to directly present the relationship between the structure of TiO_2 film and the efficiency of the solar cell, the surface morphologies of the photoanodes in flexible DSCs after different bending conditions were also observed as shown in Fig. 13. From Fig. 13, it is obviously found that the TiO_2 film cracks and even spalls off from the ITO surface after a large number of repeated outward bending. Furthermore, in order to better understand the failure mechanism of the flexible DSCs under multiple bending, the through cracks were observed by HRTEM, as shown in Fig. 14. When the bending radius is 12 mm or 9 mm, it is difficult to directly observe through cracks due to the very narrow size of the cracks and the possible zigzag morphology of the cracks. When the bending radius decreases to 8 mm and 7 mm, the through cracks (bright parts in Fig. 14) can be obviously observed.

Based on the above results and discussion, a schematic of the failure model for flexible DSCs under repeated outward bending mode was proposed as shown in Fig. 15. The photoanode of the flexible DSCs is in tension and will crack in longitudinal direction after repeated outward bending. The cracks will become through cracks with increasing the bending cycle. After that, in-plane cracks will occur and lead to localized spalling off from ITO surface (Fig. 13(e) and (f)). This will directly increase the electron transport

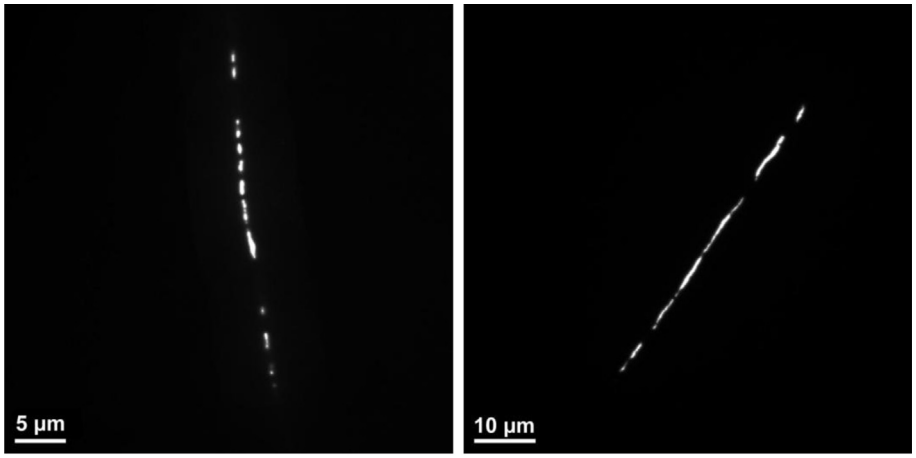

Fig. 14. HRTEM images of the through cracks after different bending conditions. The bright parts are the through cracks.

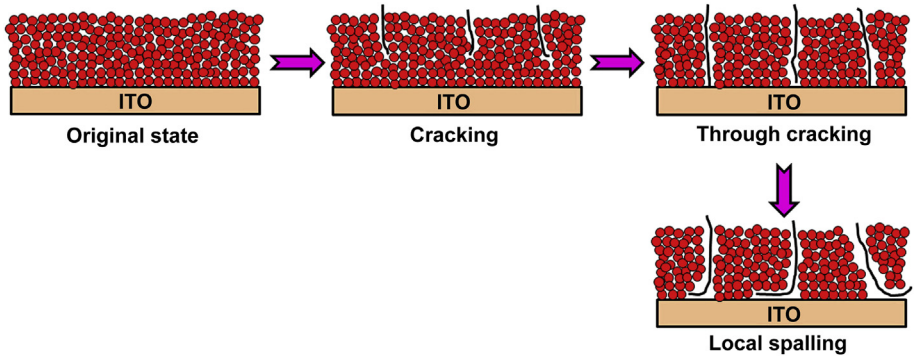

Fig. 15. Schematic of the failure model for the flexible DSCs under repeated outward bending.

difficulty from the nano-TiO_2 particles to the ITO conductive layer, and thereby decrease the electron collection efficiency and the energy conversion efficiency of the solar cell. With the repeated bending cycle, the degradation of efficiency becomes more and more severe.

4. Conclusions

The photovoltaic performance, morphology of the photoanode and electrochemical property evolution during bending service were examined to aim at understanding the bending failure mechanism for the flexible DSCs under repeated outward bending. When the bending radius was smaller than 12 mm, the efficiency of the flexible DSCs decreased with increasing the bending cycle. The decreased efficiency was mainly caused by the decrease of J_{SC} and the electron collection efficiency. The electrochemical impedance spectroscopy results showed that the increase of R_t in TiO_2 film was responsible for the degradation of efficiency. Moreover, the surface morphologies of the photoanodes after repeated bending presented cracking and spalling off of the TiO_2 film from the ITO surface. Finally, a failure model for the flexible DSCs under repeated outward bending was proposed.

Acknowledgments

The work was supported by the National Natural Science Foundation of China (No.: 51072160) and the National Program for Support of Top-notch Young Professionals.

References

[1] M. Toivola, J. Halme, K. Miettunen, K. Aitola, P.D. Lund, Int. J. Energy Res. 33 (2009) 1145–1160.
[2] H.C. Weerasinghe, P.M. Sirimanne, G.V. Franks, G.P. Simon, Y.B. Cheng, J. Photochem. Photobiol. A Chem. 213 (2010) 30–36.
[3] Y. Kijitori, M. Ikegami, T. Miyasaka, Chem. Lett. 36 (2007) 190–191.
[4] X.L. He, M. Liu, G.J. Yang, S.Q. Fan, C.J. Li, Appl. Surf. Sci. 258 (2011) 1377–1384.
[5] H. Lindstrom, A. Holmberg, E. Magnusson, S.E. Lindquist, L. Malmqvist, A. Hagfeldt, Nano. Lett. 1 (2001) 97–100.
[6] H.W. Chen, C.Y. Hsu, J.G. Chen, K.M. Lee, C.C. Wang, K.C. Huang, K.C. Ho, J. Power Sources 195 (2010) 6225–6231.
[7] D. Gutierrez-Tauste, I. Zumeta, E. Vigil, M.A. Hernandez-Fenollosa, X. Domenech, J.A. Ayllon, J. Photochem. Photobiol. A Chem. 175 (2005) 165–171.
[8] D.S. Zhang, T. Yoshida, K. Furuta, H. Minoura, J. Photochem. Photobiol. A Chem. 164 (2004) 159–166.
[9] N.G. Park, K.M. Kim, M.G. Kang, K.S. Ryu, S.H. Chang, Y.J. Shin, Adv. Mater. 17 (2005) 2349–2353.
[10] X. Li, H. Lin, J.B. Li, N. Wang, C.F. Lin, L.Z. Zhang, J. Photochem. Photobiol. A Chem. 195 (2008) 247–253.
[11] T. Kado, M. Yamaguchi, Y. Yamada, S. Hayase, Chem. Lett. 32 (2003) 1056–1057.
[12] W.H. Chiu, K.M. Lee, W.F. Hsieh, J. Power Sources 196 (2011) 3683–3687.
[13] X.L. He, G.J. Yang, H.L. Yao, C.J. Li, L. Shan, L. Mei, S.Q. Fan, Rare Metal. Mat. Eng 41 (2012) 190–194.
[14] X.L. He, G.J. Yang, C.J. Li, C.X. Li, Appl. Surf. Sci. 288 (2014) 416–422.
[15] T. Yamaguchi, N. Tobe, D. Matsumoto, T. Nagai, H. Arakawa, Sol. Energy Mater. Sol. Cells 94 (2010) 812–816.
[16] C.Y. Jiang, X.W. Sun, K.W. Tan, G.Q. Lo, A.K.K. Kyaw, D.L. Kwong, Appl. Phys. Lett. 92 (2008) 143101.
[17] Y. Li, K. Yoo, D.K. Lee, J.H. Kim, N.G. Park, K. Kim, M.J. Ko, Curr. Appl. Phys. 10 (2010) E171–E175.

[18] S.Q. Fan, G.J. Yang, C.J. Li, G.J. Liu, C.X. Li, L.Z. Zhang, J. Therm. Spray. Technol. 15 (2006) 513–517.
[19] X.L. He, M. Liu, G.J. Yang, H.L. Yao, S.Q. Fan, C.J. Li, J. Power Sources 226 (2013) 173–178.
[20] X.L. He, G.J. Yang, C.J. Li, C.X. Li, S.Q. Fan, J. Power Sources 251 (2014) 122–129.
[21] F. Fabregat-Santiago, J. Bisquert, G. Garcia-Belmonte, G. Boschloo, A. Hagfeldt, Sol. Energy Mater. Sol. Cells 87 (2005) 117–131.
[22] F. Fabregat-Santiago, J. Bisquert, E. Palomares, L. Otero, D.B. Kuang, S.M. Zakeeruddin, M. Gratzel, J. Phys. Chem. C 111 (2007) 6550–6560.
[23] W.A. MacDonald, M.K. Looney, D. MacKerron, R. Eveson, R. Adam, K. Hashimoto, K. Rakos, J. Soc. Inf. Disp. 15 (2007) 1075–1083.
[24] U. Diebold, Surf. Sci. Rep. 48 (2003) 53–229.